Interreg North Sea

Co-funded by the European Union

WaterWarmth

WORKPACKAGE 4

Smart integration of Aquathermal Energy into the local energy system

4.6 Disseminating results on system integration to local actors and to the scientific community

Version December 2025

Joyce Assaf , Mamadou-Baïlo Camara , Damien Guilbert , Brayima Dakyo
Groupe de Recherche en Electrotechnique et Automatique du Havre (GREAH)
Université Le Havre Normandie

ACCELERATING THE TRANSITION TOWARDS SUSTAINABLE HEATING AND COOLING BASED ON COLLECTIVE SURFACE WATER HEAT PUMP SYSTEM

Interreg North Sea Co-funded by the European Union
WaterWarmth

Energy Management of a Surface Water Heat Pump Powered by Wind and a Battery System

Joyce Assaf , Mamadou-Baïlo Camara , Damien Guilbert , Brayima Dakyo
Groupe de Recherche en Electrotechnique et Automatique du Havre (GREAH)
Université Le Havre Normandie
Le Havre, Normandie, France
e-mail: joyce.assaf@univ-lehavre.fr, camaram@univ-lehavre.fr, damien.guilbert@univ-lehavre.fr, brayima.dakyo@univ-lehavre.fr

Interreg North Sea Co-funded by the European Union
WaterWarmth

Abstract—The paper investigates power electronics interfaces for integrating two identical 30 kW Surface Water Heat Pumps (SWHPs) operating in parallel, with a 35 kW Wind Turbine (WT) and a 30 kWh Battery Energy Storage System (BESS), connected via a DC-bus. A simulation model was developed in MATLAB/Simulink to evaluate the behavior of the system under dynamic operating conditions, including measured data for the wind speed in 'Le Cano Ouistreham pilot site', France, and the thermal load based on data from an operational Aquathermal Energy (AE) site in Dijlemolens, Belgium. The paper addresses challenges related to efficient energy management and power control. This work presents new system-level insights, supported by simulation results. The proposed design offers flexibility and scalability, making it adaptable to integration with other Renewable Energy Sources (RESs) and a wide range of power capacities.

Keywords-Wind energy; surface water heat pump; battery energy storage system; energy management; renewable energy.

I. INTRODUCTION

Aquathermal Energy (AE) is the extraction, storage, and distribution of heat from water bodies, including surface water, wastewater, and groundwater. It is an emerging Renewable
Energy Source (RES) with strong potential for heating and cooling applications. In AE systems using surface water, heat is extracted from the water body using a Surface Water Heat Pump (SWHP) via a heat exchanger, which then increases or decreases the temperature as needed for domestic hot water
supply and other thermal energy applications [1]. AE systems reduce carbon emissions in the heating and cooling sector and decrease its reliance on imported energy [2].

According to the latest IRENA report, 87 million Heat Pumps (HPs) are projected to be installed in buildings, with wind and solar expected to contribute 91% of the total Renewable Energy (RE) capacity by 2050 [3]. When coupled with RESs, such as wind or Photovoltaics (PVs) to power their compressors, SWHPs offer a promising pathway to decarbonize the building sector [4]. In Europe, the deployment of Wind Turbines (WTs) is spreading rapidly, with wind energy accounting for almost 39% of the total electricity generated from RESs in 2024 [5]. However, due to the intermittent nature of WTs, Battery Energy Storage Systems (BESSs) are integrated to effectively manage
short-term fluctuations, while appropriate control strategies can significantly improve system reliability and efficiency [6].

Power electronics play an essential role in enabling the efficient integration of HPs with RESs. DC-links, incorporating AC-DC and DC-DC converters, allow for improved energy management, voltage regulation, and efficient power conversion across hybrid systems. Compared to traditional AC microgrids, DC-based systems offer lower conversion losses, improved energy management, and more straightforward control, particularly advantageous for hybrid configurations with large shares of DC loads or storage units [7].

In the literature, several studies have explored hybrid systems for HP applications [8]–[11]. Although these studies laid essential groundwork, they often overlooked power electronics integration, realistic thermal demand modeling, and dynamic power management between sources and loads. Few studies addressed power electronics control strategies and converter topologies for RE-powered HPs. For instance, in [12], the authors proposed an energy management strategy for a micro-grid that combines a PV, a BESS, and an air-source HP. The main goal of the study was to reduce the cost of the BESS by leveraging the thermal storage of the HP, incorporating a double fuzzy logic that coordinates power fluctuation stabilization between the BESS and the air-source HP. However, HP operation was mainly governed by RE availability and system efficiency, not by actual, time-varying thermal demand.

In [13], the authors presented a hybrid system that includes PV, WT, and BESS powering a DC-HP. However, the approach is limited as it only accounts for the electrical power consumption of the HP, with the thermal load profile being derived from thermodynamic equations without incorporating its actual dynamics. As a result, the control and performance of the system are not realistically reflective of actual HP operation, which is typically governed by unpredictable and varying thermal loads over time. Furthermore, in [14], the authors proposed an advanced control strategy based on the model predictive control combined with a fractional short-circuit current approach to optimize power extraction from the PV system interfaced with a SWHP. However, this study modeled the SWHP as a resistive load, so results were only analyzed on the PV–BESS side. Alternatively, in [15], the authors proposed a high-voltage-gain DC-DC converter to improve PV-HP coupling efficiency. Although their converter showed promising results in handling variable solar irradiance, the system also lacked realistic thermal modeling of the HP. Although their work offers valuable insights, it remains unclear whether the results are scalable to real-world scenarios.

Interreg North Sea Co-funded by the European Union
WaterWarmth

This paper contributes to the growing body of research on HPs, particularly SWHPs, by presenting a realistic simulation conducted for an AE harvesting pilot site within the "Waterwarmth" project, funded by Interreg North Sea Region, in Le Cano Ouistreham, France. This pilot site is currently in the preparatory phase for constructing a SWHP system, making it an ideal case study to simulate and validate RE integration and control strategies under realistic site conditions. The proposed system employs a 35 kW WT and a 30 kWh BESS to power two identical 30 kW SWHPs operating in parallel, all connected via a DC-bus with realistic control architecture, using both measured wind speeds and thermal load profile. The originality of this study lies in its comprehensive simulation of component interactions between fluctuating RE generation and dynamic thermal demand, and its validation of a coordinated control strategy that ensures voltage stability under realistic fluctuating wind and load conditions. The proposed model provides a more accurate reflection of operational conditions and offers a pathway toward scalable, site-adapted AE solutions.

In summary, the novelty of this work lies in three aspects: (i) the use of a measured, time-varying thermal demand profile rather than a simplified one; (ii) the coordinated control of wind and battery subsystems to ensure DC-bus stability under realistic fluctuations; and (iii) the adoption of a DC-link topology that reduces conversion stages compared to conventional AC-based systems. The main objective of this study is to design and validate, through MATLAB/Simulink simulations under real site conditions, an energy management strategy that ensures reliable demand-driven operation of a hybrid WT–BESS–SWHP system.

This paper is organized as follows: Section I briefly reviews the current state of research. Section II presents the system configuration, detailing the integrated WT, SWHP, and power electronics on both the WT and BESS sides. Subsequently, the control strategies applied to each DC-DC converter are described in Section III. Section IV presents the results of the performance analysis at a pilot site within the framework of the "Waterwarmth" project. The conclusions of this work and a paper summary are presented in Section V.

II. SYSTEM CONFIGURATION

A. Wind Turbine

The system shown in Figure 1 is based on a variable-speed WT coupled with a permanent magnet synchronous generator, which converts mechanical energy to electrical energy. The rotating rotor blades extract kinetic energy from the wind and transform it into shaft torque, which is then converted into electricity by the generator. To maximize the energy extracted from the varying wind speeds, the system relies on control strategies that regulate the WT's speed and blade pitch angle. A detailed description of the control strategy adopted is provided in Section III.

The wind speed data, which serve as input to the WT model, were collected for Le Cano Ouistreham, covering the period from March 7, 2024 at 11:00 AM to May 7, 2024 at 2:00 AM, with a sample time of one hour. This data is illustrated in Figure 2.

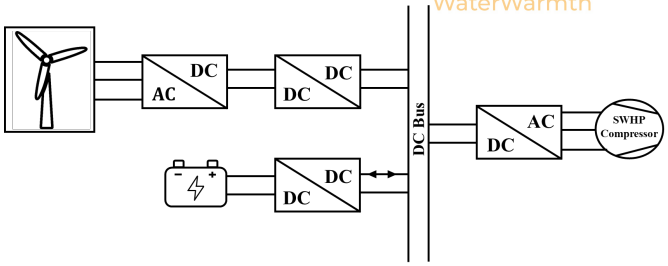

Figure 1. Electrical synoptic of the system.

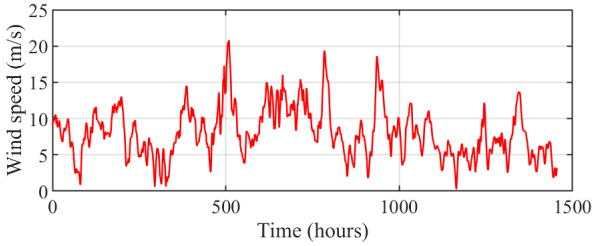

Figure 2. The wind speed profile in Le Cano Ouistreham, France.

The wind speed frequently drops below the 10.9 m/s nominal speed and occasionally falls near or below cut-in speed, reflecting the intermittent nature of wind energy. These fluctuations justify the need for both real-time WT speed control to maximize energy capture under partial load conditions and the integration of a BESS to stabilize the system's power supply.

B. Heat pump

In this model, two identical SWHPs are used as parallel loads, ensuring that the total electrical demand is closely aligned with the rated capacities of the RE generation and BESS (35 kW WT and 30 kWh BESS). This configuration also reflects the actual thermal demand of the building and removes the need for a backup gas boiler, enabling fully RE-powered operation. The SWHP considered in the simulation is a CIAT DYNACIAT LG 300 A water-to-water HP, which provides a nominal heat capacity of 90.3 kW, a cooling capacity of 61.5 kW, and a rated electrical consumption of 29.4 kW.

The primary model inputs were the thermal power generated by the SWHP (Figure 3), and its coefficient of performance (COP), based on measurements from an installed system at an operational site in Dijlemolens, Belgium. This site also uses a backup gas boiler to satisfy the total building heat demand. The data covers the period from March 7, 2024 at 11:00 AM to May 7, 2024 at 2:00 AM, with a sample time of five seconds.

The electrical power consumption for the two SWHPs is calculated based on the thermal load profile of the building, as well as the SWHP's technical datasheet. It is given by (1):

$$P_{\text{elec,SWHP}} = \frac{P_{\text{thermal}}}{COP} \quad (1)$$

Interreg North Sea Co-funded by the European Union
WaterWarmth

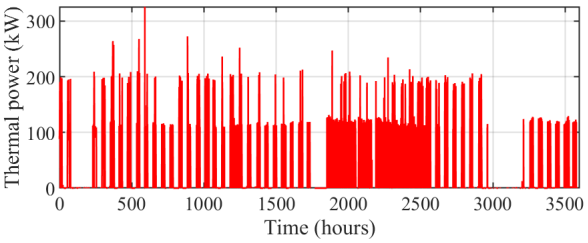

Figure 3. Thermal load profile of the SWHP.

As shown in Figure 3, the thermal load profile exhibits frequent peaks in high demand and varying on/off cycles, reflecting realistic building heating demand. Operating in a fully demand-driven mode, these dynamics emphasize the importance of a rapid control response from the supply side and a robust power balance between generation, storage, and load.

C. DC-DC boost converter on the WT side

Boost converters are commonly used in RE applications to raise the input voltage generated by the RESs, particularly when interfacing low-voltage sources, such as WTs with a higher-voltage DC-bus. In this study, the DC-bus voltage reference is 1000 V, which is a typical design choice in many RE microgrids and DC link systems, to ensure compatibility with industrial inverters and BESSs [16][17]. The converter raises the rectified WT's generated voltage to the bus voltage level, allowing efficient energy transfer under fluctuating wind conditions. Various DC-DC converter topologies are found in the literature, each with trade-offs in efficiency, control complexity, and component stress, depending on the application requirement [18]. The DC-DC boost topology used in this study is illustrated in Figure 4, with the sole purpose of validating the working principles of the overall system, providing a solid foundation for further extension and refinement.

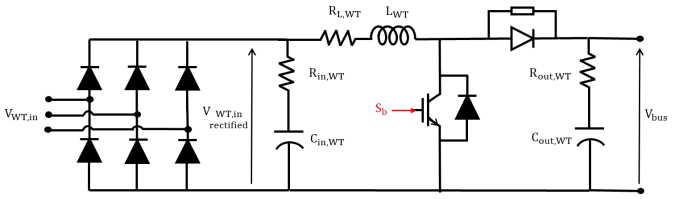

Figure 4. Topology of the AC-DC-DC converter on the WT side.

D. DC-DC bidirectional converter on the BESS side

To ensure stable operation of the DC-bus, a bidirectional buck-boost converter is implemented on the battery side. Bidirectional converters are pivotal components for energy management in RE applications, as they enable bidirectional power flow. This key feature allows excess energy generated by the RESs to be stored in the BESS during peak generation periods (buck mode) and retrieved during low-generation periods (boost mode). Therefore, their integration is vital for maximizing the utilization of RESs, as they ensure a consistent and reliable power supply. In the context of HPs, a few studies are found in the literature, including a BESS [19]. The bidirectional converter topology adopted in this study is illustrated in Figure 5 [20].

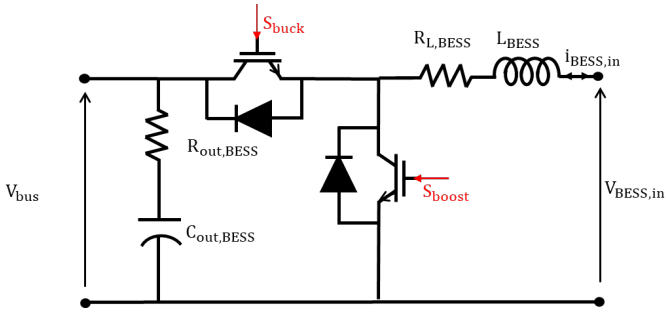

Figure 5. Topology of the AC-DC-DC converter on the WT side.

The equations governing the working principle of the buck and boost modes of this bidirectional converter are presented in (2) [21].

$$\begin{cases} \dfrac{di_{\text{BESS,in}}}{dt} = \dfrac{V_{\text{BESS,in}} - V_{\text{bus,S}_{\text{boost}}}}{L_{\text{BESS}}} \\ \dfrac{dV_{\text{bus}}}{dt} = \dfrac{i_{\text{BESS,S}_{\text{buck}}} - i_{\text{bus}}}{C_{\text{out,BESS}}} \end{cases} \tag{2}$$

where $i_{\text{BESS,in}}$ represents the current exchanged with the battery, accounting for both charging and discharging modes, V_{bus} is the measured DC-bus voltage, S_{boost} and S_{buck} are the switching signals generated by the control algorithm described in Section III, L_{BESS} is the inductance of the boost converter, and $C_{\text{out,BESS}}$ corresponds to the capacitor located at the output of the BESS, on the DC-bus side.

III. Micro-grid control methods

The control architecture of the system is designed with a clear decoupling between energy management on the source side and load operation. The SWHP functions as a passive load, turning on/off based on thermal demand. Predictive adjustment of the SWHP load is not considered; instead, the WT and the BESS are solely responsible for maintaining voltage stability and meeting demand.

A. WT Boost Converter Control Strategy

The control strategy for the WT's boost converter is based on maximizing the power extraction from the available wind-based Maximum Power Point Tracking (MPPT), while ensuring the protection of the components beyond nominal operation. Wind speed is measured and compared to a predefined nominal speed of 10.9 m/s, specific to the WT's model used. After cut-in wind speed, and if the measured wind speed is below this threshold, the reference power is computed as in (3), based on the WT power curve shown in Figure 6.

$$P = \tfrac{1}{2}\rho_{\text{air}} A C_{\text{p,max}} V_{\text{wind}}^3 \tag{3}$$

where ρ_{air} is the air density, A is the swept area of the WT blades, $C_{\text{p,max}}$ is the maximum power coefficient of the WT, and V_{wind} is the measured wind speed.

Interreg North Sea Co-funded by the European Union
WaterWarmth

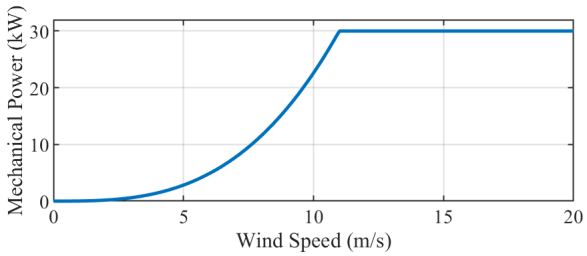

Figure 6. WT power curve.

The actual electrical power generated by the WT is measured via voltage and current sensors on the boost converter input. The power error is fed into a discrete Proportional Integral (PI) controller as illustrated in Figure 7. The error is then processed and used to generate the PWM signal for the boost converter at a switching frequency of 10 kHz, with a sample time of 10 µs.

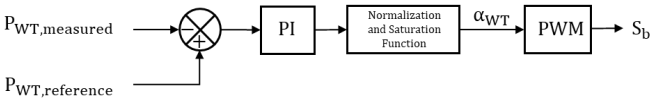

Figure 7. PWM control signal for boost switch on the WT side.

B. BESS Bidirectional Converter Control Strategy

The control of the battery-side bidirectional converter is based on maintaining the DC-bus voltage at 1000 V, while managing power flow directions (buck or boost mode) based on the instantaneous power balance between the sources and the load. For this purpose, a dual-loop bidirectional converter control was developed based on the power flow direction and the DC-bus voltage regulation. The control logic is illustrated in Figure 8 and Figure 9.

IV. Results and Discussions

The system configuration previously defined in Figure 1 is simulated in Matlab/Simulink software, with the sole purpose of validating the architecture under real operating conditions. The parameters used in the simulation are listed in Table I.

Figure 10(a) shows the performance of the DC-bus voltage control system operating in buck and boost modes. The output voltage V_{bus} closely follows the constant reference voltage of 1000 V throughout the entire operation, first reaching the target value in 3.7 seconds. Afterwards, the voltage settles within a ±5% tolerance band after approximately 1.6 seconds and remains stable, showing a reliable and steady operation. The Root Mean Square Error (RMSE) of the tracking error is about 0.42%. Although occasional transient deviations occurred, the system operated within acceptable limits, with a voltage overshoot of 4.76%, which indicates a controlled transient response without excessive voltage spikes. These results demonstrate that the controller successfully maintains the voltage regulation with minimal deviation despite mode transitions and dynamic conditions.

Figure 10(b) illustrates the performance of the WT power control loop defined in Section III. The reference curve includes

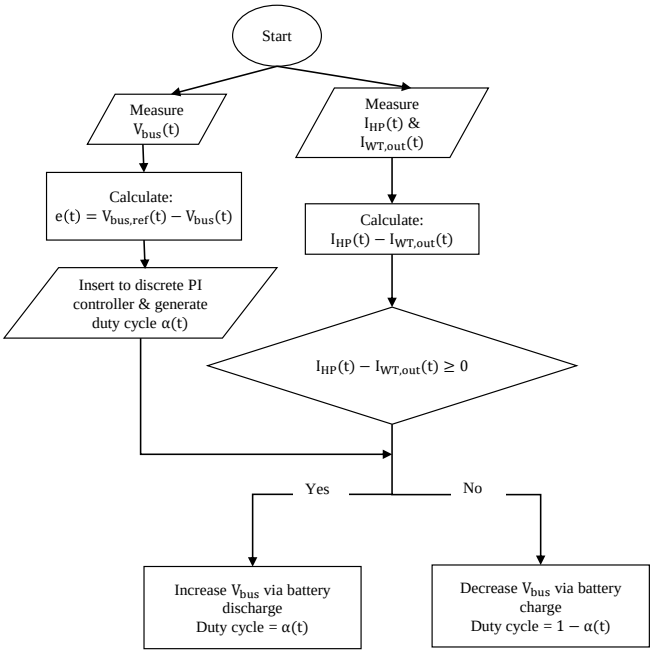

Figure 8. Buck and boost modes algorithm for the BESS bidirectional converter.

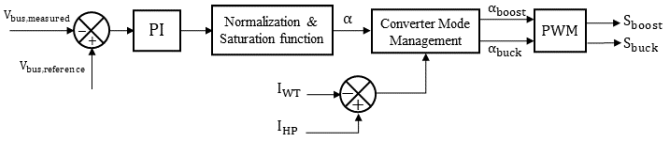

Figure 9. PWM control signals for buck and boost switches for the BESS bidirectional converter.

rapid changes and fluctuations to reflect both realistic wind and load conditions. The measured electrical power output of the WT closely follows its reference throughout the dynamic operating period, with an RMSE of almost 1.036 kW, indicating accurate and efficient tracking of the controller. Minor transient deviations occur during abrupt transitions, as expected, due to system inertia and converter response delays. However, the overall tracking behavior validates the effectiveness of the proposed control algorithm in maintaining the desired power output under varying operating conditions.

The energy management between the WT, BESS and SWHPs is illustrated in Figure 11 over an approximately 800-second simulation period. The WT output presented in Figure 11(a) fluctuates significantly between 0 and 35 kW due to wind speed variability, while the electrical power demand of the SWHPs is intermittent, varying between 0 and 52 kW, reflecting the dynamics of the thermal load profile, previously shown in Figure 3. The BESS operates bidirectionally, charging (negative power values) when the load demand is low, and discharging (positive power values) when the load demand exceeds the WT generation, as illustrated in Figure 11(b). The BESS provides up to 45 kW to maintain power balance. Therefore, the selected 100 Ah (35 kWh) battery is largely sufficient to cover the

Interreg North Sea Co-funded by the European Union
WaterWarmth

TABLE I. USED PARAMETERS IN THE SIMULATION

Simulation parameters	Values
Wind Turbine	
P_{MPPT}: Maximum power	35 kW
R: Radius	5 m
v_{nom}: Nominal wind speed	10.9 m/s
ρ_{air}: Air density	1.225 kg/m^3
C_{p}: Power coefficient	0.47
WT's Boost Converter	
$C_{\mathrm{in,WT}}$: Capacitance at rectifier's output	100 μF
$C_{\mathrm{out,WT}}$: DC-bus capacitance	3300 μF
L_{WT}: Input inductance	1 mH
$R_{\mathrm{L,WT}}$: Inductor's resistance	10 mΩ
BESS – Lithium-Ion	
V_{nom}: Nominal Voltage	350 V
Ah: Rated Capacity	100 Ah
BESS's Buck-Boost Converter	
$C_{\mathrm{out,BESS}}$: DC-bus capacitance	3300 μF
L_{BESS}: Inductance	1 mH
$R_{\mathrm{L,BESS}}$: Inductor's resistance	10 mΩ
Other parameters	
T_{s}: Sampling time	10 μs
f: Switching frequency	10 kHz

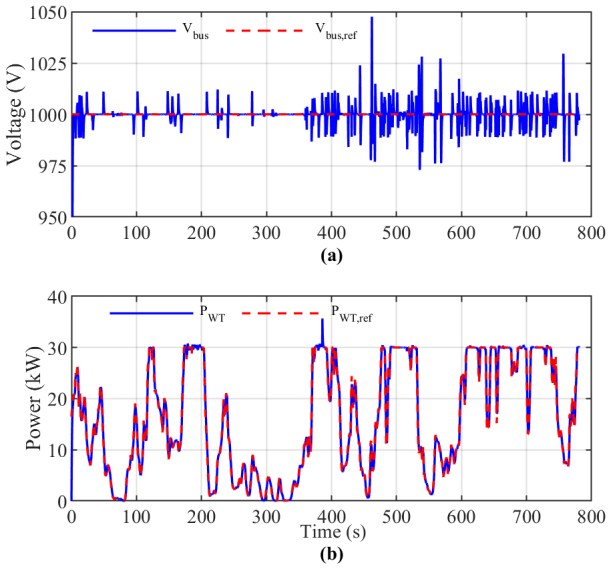

Figure 10. Comparison of measured and reference (a) DC-bus voltage (b) WT power output during control operation.

observed demand–generation imbalance under the simulated conditions. Furthermore, the overall power balance RMSE, which compares the combined generation of the WT and BESS with the electrical demand of the SWHP (Figure 11c), is almost 4 kW, indicating effective coordination between the components of the system.

Table II summarizes the key performance metrics that were derived from the simulation to quantitatively assess the dynamic performance of the proposed control strategy. These include voltage regulation accuracy, power tracking quality, and system response characteristics under variable wind speed and load conditions. The RMS tracking error represents the average percentage deviation between the measured DC-bus voltage and its reference 1000 V, computed during steady-state operation. The maximum voltage overshoot corresponds to the highest percentage by which the DC-bus voltage exceeds its reference during dynamic transients. The settling time is the duration required for the measured DC-bus voltage to return and remain within ±5% of its reference after a significant disturbance.

The simulation results confirm that the WT–BESS mix reliably tracks the HP's dynamic demand, validating control strategies under real-time conditions. In addition, the proposed DC-based architecture reduces conversion stages, achieving 95–96% efficiency—about 3–5% higher than conventional AC systems.

V. Conclusion and Future Work

In this study, a hybrid system consisting of a Wind Turbine (WT), Battery Energy Storage System (BESS), and two Surface Water Heat Pumps (SWHPs) was developed. A complete description of the components of the proposed system is presented, along with the physical model associated with these components. The proposed control methods and their features

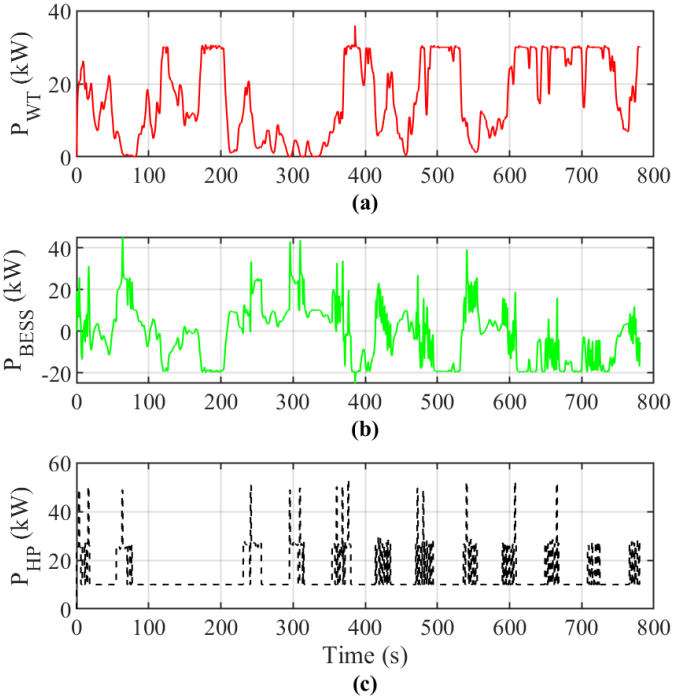

Figure 11. Instantaneous power profiles of the WT, BESS, and HP.

TABLE II. System Control Performance Metrics

Metric	Value
RMS voltage tracking error of DC-bus voltage	0.42%
Max voltage overshoot of DC-bus voltage	4.76%
Settling time of DC-bus voltage	1.6 s
WT electric power tracking RMSE	1.036 kW
Power balance RMSE	3.981 kW

Interreg North Sea Co-funded by the European Union
WaterWarmth

are then highlighted. The simulation results demonstrated that the proposed control strategy achieves a fast dynamic response, stable voltage regulation, and accurate power tracking performance. This study is a proof of the feasibility and effectiveness of using such hybrid configurations to power thermal systems in a sustainable manner, offering scalable and site-adaptable solutions. Although the present study relied on classical PI-based control loops to validate feasibility, future work will investigate more innovative control strategies, such as model predictive controllers, in combination with alternative DC–DC converter topologies, to further enhance dynamic performance and robustness.

ACKNOWLEDGMENT

This work is done at GREAH-laboratory, University of Le Havre Normandie, particularly by the research team based renewable energies and storage systems (MERS). This work is done within the framework of Interreg Waterwarmth project co-funded by the European Union. The authors would like to thank the European Union and the University of Le Havre Normandie for their financial support.

REFERENCES

[1] J. D. Spitler and M. S. Mitchell, "Surface Water Heat Pump Systems", in *Advances in Ground-Source Heat Pump Systems*, Elsevier, 2016, pp. 225–246.

[2] E. Brasser, "Heating Houses using Surface Water: A Sustainable Alternative to Natural Gas", Ph.D. dissertation, Delft University of Technology, Delft, Netherlands, 2020.

[3] International Renewable Energy Agency (IRENA), "Regional Energy Transition Outlook: European Union", IRENA, Abu Dhabi, Report, 2025. DOI: ISBN:978-92-9260-658-9.

[4] A. Żelazna and A. Pawłowski, "Review of the Role of Heat Pumps in Decarbonization of the Building Sector", *Energies*, vol. 18, no. 13, 2025, ISSN: 1996-1073. DOI: 10.3390/en18133255.

[5] Eurostat, *Net electricity generation by type of fuel – monthly data*, [Online], Accessed: Jul. 07, 2025, 2025.

[6] D. Rekioua, "Hybrid Renewable Energy Systems Overview", in *Hybrid Renewable Energy Systems: Optimization and Power Management Control*, Springer, 2019, pp. 1–37.

[7] N. Bayati, A. Hajizadeh, and M. Soltani, "Protection in DC Microgrids: A Comparative Review", *IET Smart Grid*, vol. 1, no. 3, pp. 66–75, 2018. DOI: 10.1049/iet-stg.2018.0024.

[8] S. Baraskar, D. Günther, J. Wapler, and M. Lämmle, "Analysis of the Performance and Operation of a Photovoltaic-Battery Heat Pump System Based on Field Measurement Data", *Solar Energy Advances*, vol. 4, p. 100 047, 2024. DOI: 10.1016/j.seadv.2023.100047.

[9] A. V. Klokov, A. S. Tutunin, E. S. Sharaborova, A. A. Korshunov, and E. Y. Loktionov, "Inverter Heat Pumps as a Variable Load for Off-Grid Solar-Powered Systems", *Energies*, vol. 16, no. 16, p. 5987, 2023, ISSN: 1996-1073. DOI: 10.3390/en16165987.

[10] M. Bojić, N. Nikolić, D. Nikolić, J. Skerlić, and I. Miletić, "Toward a Positive-Net-Energy Residential Building in Serbian Conditions", *Applied Energy*, vol. 88, no. 7, pp. 2407–2419, 2011, ISSN: 0306-2619. DOI: 10.1016/j.apenergy.2011.01.015.

[11] C. Roselli, M. Sasso, and F. Tariello, "Dynamic simulation of a solar electric driven heat pump for an office building located in southern italy", *International Journal of Heat and Technology*, vol. 34, no. S2, S496–S504, 2016, ISSN: 0392-8764. DOI: 10.18280/ijht.34S243.

[12] L. Yang, N. Tai, C. Fan, and Y. Meng, "Energy Regulating and Fluctuation Stabilizing by Air Source Heat Pump and Battery Energy Storage System in Microgrid", *Renewable Energy*, vol. 95, pp. 202–212, 2016, ISSN: 0960-1481. DOI: 10.1016/j.renene.2016.04.026.

[13] C. B. N. Fapi, M. L. Touré, M.-B. Camara, and B. Dakyo, "Control Strategy for DC Micro-Grids in Heat Pump Applications with Renewable Integration", *Electronics*, vol. 14, no. 1, p. 150, 2025, ISSN: 2079-9292. DOI: 10.3390/electronics14010150.

[14] C. B. N. Fapi, M. L. Touré, M.-B. Camara, and B. Dakyo, "MPPT Based Fractional Short-Circuit Current-Model Predictive Control for PV System in Real Weather Conditions for Heat-Pump Applications", in *Proc. of the 2024 International Conference on Intelligent Systems and Computer Vision (ISCV)*, IEEE, 2024, pp. 1–6. DOI: 10.1109/ISCV61718.2024.10694395.

[15] C. B. N. Fapi, M. L. Touré, M.-B. Camara, and B. Dakyo, "High Voltage Gain DC-DC Converter Based Maximum Power Tracking from Photovoltaic Systems for Heat-Pump Applications", in *Proc. of the 2024 12th International Conference on Smart Grid (icSmartGrid)*, IEEE, 2024, pp. 493–498. DOI: 10.1109/icSmartGrid61521.2024.10557289.

[16] K. B. Samal, S. Pati, and R. Sharma, "Power Management Using an Improved EMS Algorithm in a Stand-Alone Hybrid PV-PEMFC Microgrid with Reduced Converter Count", *Green Energy and Intelligent Transportation*, p. 100 302, 2025, ISSN: 2772-3755. DOI: 10.1016/j.get.2025.100302.

[17] K. Zafar, M. K. Kamaludeen, Y. Esa, A. A. A. Mohamed, and S. Odie, "Fault analysis for dc bus-integrated energy storage system, electric vehicle supply equipment, and photovoltaic systems", *Electric Power Systems Research*, vol. 234, p. 110 837, 2024. DOI: 10.1016/j.epsr.2024.110837.

[18] J. Assaf, J. S. Menye, M. B. Camara, D. Guilbert, and B. Dakyo, "Power Converter Topologies for Heat Pumps Powered by Renewable Energy Sources: A Literature Review", *Electronics*, vol. 13, no. 19, p. 3965, 2024, ISSN: 2079-9292. DOI: 10.3390/electronics13193965.

[19] C. Lorenzo, L. Narvarte, R. H. Almeida, and A. B. Cristóbal, "Technical Evaluation of a Stand-Alone Photovoltaic Heat Pump System Without Batteries for Cooling Applications", *Solar Energy*, vol. 206, pp. 92–105, 2020, ISSN: 0038-092X. DOI: 10.1016/j.solener.2020.05.051.

[20] M. B. Camara, "Supercapacitors for Dynamic Energy Exchange Onboard Hybrid Electric Vehicles: Modeling, Converter Study, and Control", English, PhD Thesis, Université de Franche-Comté, France, 2007.

[21] S. Agrawal, L. Umanand, and B. S. Reddy, "Bidirectional Current-Fed Converter for High Gain DC–DC and DC–AC Applications", in *Proc. of the Symposium on Power Electronic and Renewable Energy Systems Control (PERESC 2020)*, ser. Lecture Notes in Electrical Engineering, vol. 731, Singapore: Springer, 2021, pp. 101–111. DOI: 10.1007/978-981-33-4081-9_10.